The Role of Ammonia in the Distribution of Volatiles in the Primordial Hydrosphere of Europa

Alizée Amsler Moulanier, Olivier Mousis, Alexis Bouquet, Christopher R Glein

The Planetary Science Journal, 6:1 (12pp), 2025 January https://doi.org/10.3847/PSJ/ad9925

The Role of Ammonia in the Distribution of Volatiles in the Primordial Hydrosphere of Europa

Alizée Amsler Moulanier[1,5], Olivier Mousis[1,2], Alexis Bouquet[3,1], and Christopher R. Glein[4]
[1] Aix-Marseille Université, CNRS, CNES, Institut Origines, LAM, Marseille, France
[2] Institut Universitaire de France (IUF), France
[3] Aix-Marseille Université, CNRS, Institut Origines, PIIM, Marseille, France
[4] Space Science Division, Space Sector, Southwest Research Institute, 6220 Culebra Road, San Antonio, TX 78238-5166, USA
Received 2024 July 17; revised 2024 November 27; accepted 2024 November 27; published 2025 January 2

Abstract

The presence of a hydrosphere on Europa raises questions about its habitability, and studies of its volatile inventory can provide insight into its formation process. Different scenarios suggest that Europa's volatiles could be derived from cometary ices or devolatilized building blocks. The study of post-accretion processes—in particular, the "open-ocean" phase that likely occurred before the formation of the icy crust—is crucial to distinguishing these origins, as this phase is likely to have influenced the volatile inventory. The abundance of ammonia in Europa's building blocks is also crucial for understanding the composition of its ocean and primordial atmosphere. We aim to investigate the ocean–atmosphere equilibrium during the post-accretion period by varying the ammonia fraction in the atmosphere. Our model evaluates the vapor–liquid equilibrium of water and volatiles, as well as the chemical equilibrium within the ocean, to study Europa's early hydrosphere. We explore two initial conditions: one in which Europa's hydrosphere originates from comet-like building blocks, and another in which it forms in equilibrium with a thick-and-CO_2-rich atmosphere. In both scenarios, the initial ratio of accreted CO_2 to NH_3 determines the magnitude of their partial pressures in Europa's early atmosphere. If this ratio exceeds a certain threshold (set to 10^{-4} in this study), the atmosphere will be CO_2-rich; otherwise, it will be CO_2-depleted, by multiple orders of magnitude. Overall, our work provides an initial assessment of the distribution of primordial volatiles in Europa's primitive hydrosphere and provides a baseline for interpreting data from the upcoming Europa Clipper mission.

Unified Astronomy Thesaurus concepts: Planetary science (1255); Galilean satellites (627); Ocean-atmosphere interactions (1150); Natural satellite formation (1425); Europa (2189)

1. Introduction

Jupiter's moon Europa harbors a vast global subsurface ocean beneath its icy outer shell (K. K. Khurana et al. 1998; R. T. Pappalardo et al. 1999; M. G. Kivelson et al. 2000). This ocean is likely in contact with the moon's silicate mantle, potentially facilitating hydrothermal processes (M. Y. Zolotov et al. 2009). Interactions between the liquid water and the surface of the icy crust are anticipated, contributing to the exchange of endogenous materials. Indeed, Europa's average surface is young (E. B. Bierhaus et al. 2009), and the presence of salts on disrupted areas of Europa's surface could be indicative of such processes (T. B. McCord et al. 2002; J. Dalton et al. 2005).

The circumstances surrounding Europa's formation remain a subject of ongoing interest, especially concerning the origin of its water content (~8 wt%; G. Schubert et al. 2004; L. Gomez Casajus et al. 2021), which could derive from different types of accreted material and source locations. Europa's volatile content might have come directly from the circumplanetary disk (CPD), where its building blocks could have condensed in situ (R. G. Prinn & B. J. Fegley 1981). Another possibility is that Europa's volatiles originated in the protosolar nebula (PSN), where its building blocks formed before entering the Jovian CPD and subsequently accreting onto the Galilean moons (R. M. Canup & W. R. Ward 2002; O. Mousis & D. Gautier 2004; T. Ronnet et al. 2018). Moreover, water could have been brought to Europa through different processes. An accretion of a mixture of hydrated rocks and ice is a plausible scenario modeled in R. M. Canup & W. R. Ward (2002) and T. Ronnet et al. (2017). On the other hand, after carbonaceous chondrites' dehydration, the accretion process could also be at the origin of Europa's hydrosphere (M. Melwani Daswani et al. 2021; O. Mousis et al. 2023; K. T. Trinh et al. 2023).

Understanding the processes related to the early stages of Europa's evolution is crucial for deducing the moon's formation history based on its present composition. It is conceivable that shortly after its accretion, Europa existed in an "open-ocean" configuration, where a dense atmosphere coexisted and chemically equilibrated with the global ocean (J. I. Lunine & D. J. Stevenson 1987; J. I. Lunine & M. C. Nolan 1992). In time, such a configuration would evolve to the "closed-ocean" one, observable nowadays, where the global ocean is covered by an ice crust. As the current composition of Europa's subsurface ocean may be intrinsically linked to the "open-ocean" one, it is crucial to retrace the evolution of the hydrosphere. The coupling of the modeling of how volatiles were distributed during the "open-ocean" phase with the future detection of compounds indicative of the subsurface ocean's current composition could provide valuable insights into the evolution of the volatile content possibly sequestered in Europa's contemporary hydrosphere (global ocean and ice crust). However, the volatile content incorporated into Europa's ocean after accretion is contingent on the type of accreted

[5] Corresponding author.

material and thus the moon's formation conditions. As a consequence, through the exploration of this early "open-ocean" phase in Europa's history, we intend to quantify the consequences of different formation scenarios on the evolution of the volatile content of Europa's hydrosphere and to anticipate future additions to compositional data from ESA's JUICE and NASA's Europa Clipper missions (R. T. Pappalardo et al. 2024).

Observations of Europa's surface have led to suspicions about the presence of compounds such as CO_2, likely of endogenic origin (S. K. Trumbo & M. E. Brown 2023; G. L. Villanueva et al. 2023), sulfates (C. Hibbitts et al. 2019), and Mg-chlorinated salts (N. Ligier et al. 2016) within the ocean. While not yet detected, it is important to assess the distribution of nitrogen-bearing species. These species can significantly influence habitability conditions, N being one of the essential elements for building life as we know it. One relevant nitrogen-bearing species worth studying is ammonia, which is abundant in cometary ices (D. Bockelée-Morvan & N. Biver 2017). Consequently, it is presumed to be present among the nitrogen-bearing species found on icy worlds. NH_3 is also frequently cited as an antifreeze in the oceans of icy moons (O. Grasset & C. Sotin 1996; M. Neveu et al. 2017; K. T. Trinh et al. 2023), so it could play a role in maintaining their liquid state.

Moreover, NH_3 can influence the pressure distribution within the primordial atmosphere. As CO_2 and NH_3 react in water, their speciation products—which are respectively acidic and basic—will engage in acid–base reactions. These ionic forms are more soluble than their neutral counterparts, suggesting that the chemical equilibrium may shift based on whether CO_2 or NH_3 predominates. As a result, depletion of either CO_2 or NH_3 in the liquid phase would cause the partial pressure distribution in the gas phase to adjust accordingly. In addition, experimental evidence has shown a correlation between the dissolved CO_2–NH_3 ratio and the partial pressure distribution in the H_2O–CO_2–NH_3 system's liquid–vapor equilibrium (D. W. Van Krevelen et al. 1949; U. Gppert & G. Maurer 1988; V. Bieling et al. 1989). Previous studies, such as M. Melwani Daswani et al. (2021), predicted the existence of a thick CO_2 primordial atmosphere for Europa. However, those models did not incorporate ammonia or nitrogen in the primordial bulk composition of the moon. We aim to explore how the presence of ammonia impacts the initial distribution of volatiles in the primordial hydrosphere. The amount and chemical forms of nitrogen delivered to Europa during its formation depend on the composition of the materials accreted throughout its growth phase. Nitrogen compounds, although present in different concentrations, have been detected in both carbonaceous chondrites and cometary ice (G. Marion et al. 2012; S. Pizzarello & L. B. Williams 2012; M. Rubin et al. 2019). In this study, we examine two scenarios for the composition of Europa's primordial atmosphere. Both scenarios assume that the atmospheric reservoir outgassed from the interior due to vigorous accretional and radiogenic heating, reaching equilibrium with an underlying liquid ocean (J. I. Lunine & D. J. Stevenson 1987; C. J. Bierson & F. Nimmo 2020). The first scenario assumes a comet-like atmospheric composition resulting from the outgassing of building blocks that originated in the PSN (R. M. Canup & W. R. Ward 2002; O. Mousis & D. Gautier 2004; T. Ronnet et al. 2017). The second scenario posits a primordial, CO_2-rich atmosphere formed after Europa's accretion, as established by M. Melwani Daswani et al. (2021).

To highlight the implications of such a choice on the initial distribution of volatiles in the early phase of the moon, we followed the approach of N. Marounina et al. (2018) by developing a model designed to calculate the volatile partitioning between the ocean and the atmosphere. This model takes into account the liquid–vapor equilibrium between the two phases and is coupled with chemical equilibrium in the liquid phase. We employ this model to evaluate the extent to which the initial distribution of volatiles—particularly CO_2 and NH_3 content—influences the equilibrium between the primordial atmosphere and ocean.

The paper proceeds as follows. Section 2 is devoted to a description of the model used in this study to compute the distribution of volatiles between an ocean and an atmosphere. In Section 3, we first show the proportion of volatiles in early Europa's hydrosphere, for the specific case where Europa's water content was brought by cometary ice, and explore how the amount of incorporated ammonia may shift this equilibrium. Then, the equilibrium that would result starting from a primordial CO_2-rich atmosphere is computed as well. In Section 4, we discuss the implications of our results in the context of the current state of knowledge about Europa. Finally, our results are summarized in Section 5 and their outcomes along with additional processes to be considered are discussed.

2. Model Description

The model used in this study, summarized in Figure 1, focuses on the dissolution of volatiles in a water ocean at a shallow depth. Two thermodynamic phases—the primordial atmosphere and the ocean—are in equilibrium, and the dissolved gases are considered as aqueous species. Temperature is a user input and assumed to be constant at the ocean–atmosphere interface, within a range of temperatures possible at the surface after accretion (G. Schubert et al. 1981; C. J. Bierson & F. Nimmo 2020). The approach involves initiating the volatile species into the atmosphere, acting as a primordial reservoir in equilibrium with the ocean during its early open phase. This is justified by the fact that, immediately after accretion, the atmosphere formed through outgassing releases a substantial portion of the volatiles initially present in Europa's building blocks into the atmosphere (J. I. Lunine & M. C. Nolan 1992; M. Melwani Daswani et al. 2021). Atmospheric escape is not considered in this study. We focus on the interface between the atmosphere and the ocean. The nonideal behaviors and interactions of volatiles in the atmosphere and the ocean are accounted for by computing fugacity and activity coefficients. The equilibrium between the two phases is coupled to a chemical equilibrium model, in which the speciation of the two most reactive species—carbon dioxide and ammonia—is considered. The modeled chemical system is simplified, in order to understand the general features of its chemistry. Species such as O_2, CO, CH_4, and N_2 are not taken into account, due to either their low reactivity in water or because the conditions for chemical reactions to happen are not met in this modeling (for CO oxidation, see, for instance, J. S. Seewald et al. 2006). They are present, however, in the liquid–vapor equilibrium. We also do not consider any water–rock reactions involving Europa's silicate mantle and ocean. The description of the model is split into two subsections: the

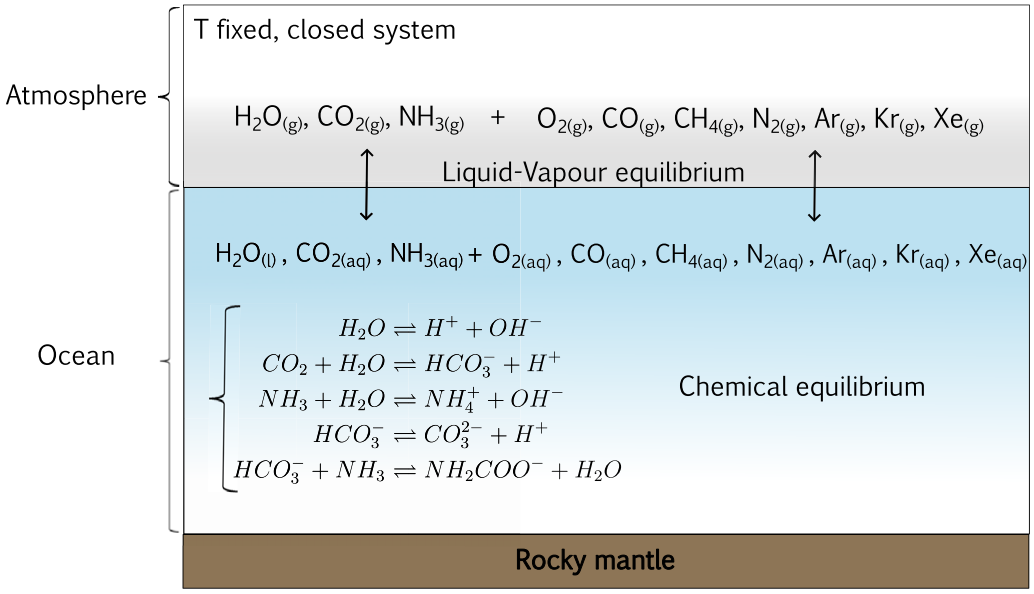

Figure 1. Model scheme representation. The model represents the dissolution of volatiles from the primordial atmosphere into the ocean. The liquid–vapor equilibrium of the volatile species is coupled to a chemical equilibrium model that considers the speciation of H_2O, CO_2, and NH_3. This coupled approach allows the partitioning of the volatiles between the atmosphere and the ocean to be determined, taking into account both physical and chemical equilibrium. This model does not account for water–rock interactions between the ocean and silicate mantle.

first is focused on the liquid–vapor equilibrium and the second on the chemical speciation within the ocean.

2.1. Liquid–Vapor Equilibrium

We first introduce the equations for phase equilibrium. The liquid–vapor equilibrium for each species is set by the equality between the vapor and liquid phases' fugacities, f_i^V and f_i^L, respectively:

$$f_i^V(T, P, y_i) = f_i^L(T, P, x_i). \tag{1}$$

Here, the fugacity of the species i in the vapor phase, f_i^V, is a function of the temperature T, pressure P, and the mole fraction y_i in the vapor phase. Similarly, the fugacity of the species i in the liquid phase, f_i^L, is a function of T, P, and the mole fraction x_i in the liquid phase.

This equation represents Raoult's law, which describes the equilibrium between the vapor and liquid phases for a given species. By enforcing this equality, the model can determine the partitioning of volatiles between the atmosphere and the ocean.

By introducing the fugacity coefficient ϕ and the activity coefficient γ, the fugacity of each phase for an individual species i can be written as:

$$\begin{aligned} f_i^V &= \phi_i y_i P, \\ f_i^L &= \gamma_i x_i f_i^0. \end{aligned} \tag{2}$$

In the vapor phase, the fugacity f_i^V is a function of the fugacity coefficient ϕ_i, the mole fraction y_i, and the total pressure P in Pascal. This expression accounts for the nonideal behavior of the gas phase. In the liquid phase, the fugacity f_i^L is a function of the activity coefficient γ_i, the mole fraction x_i, and the standard-state fugacity f_i^0. The activity coefficient γ_i captures the nonideal interactions between the dissolved species in the liquid phase.

By substituting these expressions into Equation (1), the model can determine the partitioning of volatiles between the atmosphere and the ocean, taking into account the nonideal behaviors of both phases. The standard-state fugacity f_i^0 of H_2O is set to the saturation pressure of water, $P_{H_2O}^{sat}(T)$, which is calculated using the Antoine equation (D. R. Stull 1947):

$$\log_{10}(P_{H_2O}^{sat}) = A - \frac{B}{T + C}, \tag{3}$$

with $A = 4.6543$, $B = 1435.264$, $C = -64.848$, T in kelvins, and P in bar.

Equation (2) can then be rewritten as:

$$\begin{aligned} \phi_{H_2O}\ P\ y_{H_2O} &= \gamma_{H_2O}\ x_{H_2O}\ P_{H_2O}^{sat}(T) \\ \phi_i P y_i &= \gamma_i\ x_i\ H_{H_2O,i}(T) \exp\left(\frac{v_{i,H_2O}^{\infty}(P - P_{H_2O}^{sat})}{RT}\right), \end{aligned} \tag{4}$$

where the standard-state fugacity f_i^0 of dissolved species i is approximated as the Henry's law constant, corrected by a Poynting factor (K. Kawazuishi & J. M. Prausnitz 1987; V. Darde et al. 2010). The Henry's law constants and their temperature dependencies are reported in Table 1 and were taken from K. Kawazuishi & J. M. Prausnitz (1987), for CO_2 and NH_3, and from P. Warneck & J. Williams (2012) for the other species.

The molar volume of the species i at infinite dilution, v_{i,H_2O}^{∞}, is extrapolated from B. Rumpf & G. Maurer (1993a, 1993b) and J. E. Garcia (2001), for CO_2 and NH_3. For the other species, v_{i,H_2O}^{∞} is set to 0. R is the ideal gas constant.

Following other studies in the same pressure–temperature range (G. Pazuki et al. 2006; N. Marounina et al. 2018), we compute the fugacity coefficient ϕ_i for each species using the Peng–Robinson equation of state (EOS; D.-Y. Peng & D. B. Robinson 1976) and the Van der Waals one-fluid mixing rule. The molar volume of the mixture v is derived from the Peng–Robinson EOS:

$$P = \frac{RT}{v - b} - \frac{a\alpha}{v^2 + 2vb - b^2}, \tag{5}$$

Table 1
Henry's Constant Interpolation Formulas of Gases in Water

Molecule	Henry's Constant Formula	Unit
CO_2[a]	$\ln(H_i) = -17060.71/T - 68.31596 \ln T + 0.06598907T + 430.1920$	$bar.kg.mol^{-1}$
NH_3[a]	$\ln(H_i) = -7579.948/T - 13.58857 \ln T + 0.008596972T + 96.23184$	$bar.kg.mol^{-1}$
O_2[b]	$\ln(H_i) = -175.33 + 8747.5/T + 24.453 \ln T$	$mol.dm^{-3}.atm^{-1}$
CO[b]	$\ln(H_i) = -178.00 + 8750.0/T + 24.875 \ln T$	$mol.dm^{-3}.atm^{-1}$
CH_4[b]	$\ln(H_i) = -211.28 + 10447.9/T + 29.780 \ln T$	$mol.dm^{-3}.atm^{-1}$
N_2[b]	$\ln(H_i) = -177.57 + 8632.1/T + 24.798 \ln T$	$mol.dm^{-3}.atm^{-1}$
Ar[b]	$\ln(H_i) = -146.40 + 7479.3/T + 20.140 \ln T$	$mol.dm^{-3}.atm^{-1}$
Kr[b]	$\ln(H_i) = -174.52 + 9101.7/T + 24.221 \ln T$	$mol.dm^{-3}.atm^{-1}$
Xe[b]	$\ln(H_i) = -197.21 + 10521.0/T + 27.466 \ln T$	$mol.dm^{-3}.atm^{-1}$

Notes.
[a] K. Kawazuishi & J. M. Prausnitz (1987).
[b] P. Warneck & J. Williams (2012).

where

$$a = \frac{0.457235R^2T_c^2}{P_c},$$
$$b = \frac{0.077796RT_c}{P_c},$$
$$\alpha = \left(1 + \kappa\left(1 - \sqrt{\frac{T}{T_c}}\right)\right)^2,$$
$$\text{and} \quad \kappa = 0.37464 + 1.54226\omega - 0.2699\omega^2. \tag{6}$$

Here, T_c is the critical temperature, P_c is the critical pressure, and ω is the acentric factor of each volatile. Their values are displayed in Table 2.

The mixture parameters A_{mix} and B_{mix} required for the Peng–Robinson EOS and the Van der Waals one-fluid mixing rule are computed using the following equations:

$$A_i = a_i \times \alpha_i,$$
$$A_{ij} = (1 - k_{ij})\sqrt{A_iA_j},$$
$$A_{\text{mix}} = \sum_i^N \sum_j^N y_i y_j A_{ij},$$
$$\text{and} \quad B_{\text{mix}} = \sum_i^N y_i b_i, \tag{7}$$

where N is the total number of species. α_i, a_i, and b_i are computed for each species i using Equation (6). When available, binary interaction coefficients k_{ij} are used to further account for the nonideal interactions between the volatile species, following the approach described in K. Gasem et al. (2001). If not, they are set to 0. These binary interaction coefficients are determined empirically and taken from the literature (A. Dhima et al. 1999, for H_2O–CO_2; J. Vrabec et al. 2009 for the other couples). By incorporating these binary interaction coefficients, the model can more accurately capture the nonideal behaviors of the volatile mixtures in the atmosphere and ocean.

After having computed the molar volume v from the Peng–Robinson EOS (Equation (5)), the fugacity coefficient ϕ_i of a species i can be derived from Equation (5):

Table 2
T_c, P_c, and ω Values Used in the Model (R. Reid et al. 1987)

Molecule	T_c	P_c	ω
H_2O	647.3	220.6	0.3434
CO_2	304.19	73.83	0.224
NH_3	405.6	112.8	0.25
O_2	154.4	50.5	0.022
CO	132.9	35.0	0.066
CH_4	190.4	46.0	0.011
N_2	126.3	33.9	0.039
Ar	150.8	48.7	0.001
Kr	209.4	55.0	0.005
Xe	289.7	58.4	0.008

$$\ln(\phi_i(T, v, y)) = \frac{b_i}{B_{\text{mix}}}(Z - 1) - \ln\left[\frac{P}{RT}(v - B_{\text{mix}})\right]$$
$$\text{with} \quad + \frac{A_{\text{mix}}}{2\sqrt{2}RTB_{\text{mix}}} \ln\left(\frac{v - B_{\text{mix}}2.414}{v - B_{\text{mix}}0.414}\right)\left(\delta_i - \frac{b_i}{B_{\text{mix}}}\right), \tag{8}$$
$$Z = \frac{Pv}{RT}, \qquad \delta_i = 2\frac{A_i}{A_{mix}}\sum_j y_j\sqrt{A_j}(1 - k_{ij}). \tag{9}$$

The activity coefficients of H_2O, CO_2, and NH_3 are computed with the extended UNIQUAC model (K. Thomsen & P. Rasmussen 1999). The activity coefficient of CH_4 is taken from B. Kvamme (2021). For the other neutral species, we set $\gamma_i = 1$.

2.2. Chemical Equilibrium

In this model, we couple the liquid–vapor equilibrium with the chemical equilibrium taking place within the aqueous H_2O–CO_2–NH_3 system:

$$H_2O \rightleftharpoons H^+ + OH^-, \tag{10}$$
$$CO_2 + H_2O \rightleftharpoons HCO_3^- + H^+, \tag{11}$$
$$NH_3 + H_2O \rightleftharpoons NH_4^+ + OH^-, \tag{12}$$
$$HCO_3^- \rightleftharpoons CO_3^{2-} + H^+, \tag{13}$$
$$HCO_3^- + NH_3 \rightleftharpoons NH_2COO^- + H_2O. \tag{14}$$

The equations describing the chemical equilibrium within the H_2O–CO_2–NH_3 system are derived from the dissociation

reactions of these species:

$$K_{H_2O} = \frac{m_{OH^-} m_{H^+}}{x_{H_2O}} \frac{\gamma_{OH^-}\gamma_{H^+}}{\gamma_{H_2O}}, \quad (15)$$

$$K_{CO_2} = \frac{m_{HCO_3^-} m_{H^+}}{x_{H_2O} m_{CO_2}} \frac{\gamma_{HCO_3^-}\gamma_{H^+}}{\gamma_{H_2O}\gamma_{CO_2}}, \quad (16)$$

$$K_{NH_3} = \frac{m_{NH_4^+} m_{OH^-}}{x_{H_2O} m_{NH_3}} \frac{\gamma_{NH_4^+}\gamma_{OH^-}}{\gamma_{H_2O}\gamma_{NH_3}}, \quad (17)$$

$$K_{HCO_3^-} = \frac{m_{CO_3^{2-}} m_{H^+}}{m_{HCO_3^-}} \frac{\gamma_{CO_3^{2-}}\gamma_{H^+}}{\gamma_{HCO_3^-}}, \quad (18)$$

$$K_{NH_2COO^-} = \frac{m_{NH_2COO^-} x_{H_2O}}{m_{NH_3} m_{HCO_3^-}} \frac{\gamma_{NH_2COO^-}\gamma_{H_2O}}{\gamma_{NH_3}\gamma_{HCO_3^-}}, \quad (19)$$

where $K_i(T)$ is the dissociation constant of each reaction, taken from K. Kawazuishi & J. M. Prausnitz (1987), m_i (in moles per kilogram) is the molality of the aqueous species, x_{H_2O} is the mole fraction of water, and γ_i is the activity coefficient of the species i.

The activity coefficients involved in the chemical equilibrium equations are computed using the extended UNIQUAC model, first introduced in K. Thomsen & P. Rasmussen (1999), and the parameters of V. Darde et al. (2010). This model calculates the activity coefficient using combinatorial, residual, and electrostatic terms, with the latter based on the extended Debye–Hückel law. It is well established for studying this specific chemical equilibrium (K. Thomsen & P. Rasmussen 1999; K. Thomsen 2005; V. Darde et al. 2010). Finally, to retrieve the whole set of variables, the mass and charge-balance equations are derived as follows:

$$x_{CO_{2tot}} = x_{CO_2} + x_{HCO_3^-} + x_{CO_3^{2-}} + x_{NH_2COO^-}, \quad (20)$$

$$x_{NH_{3tot}} = x_{NH_3} + x_{NH_4^+} + x_{NH_2COO^-}, \quad (21)$$

$$x_{H^+} + x_{NH_4^+} = x_{OH^-} + x_{HCO_3^-} + 2x_{CO_3^{2-}} + x_{NH_2COO^-}, \quad (22)$$

where $x_{CO_{2tot}}$ and $x_{NH_{3tot}}$ are the total mole fractions of CO_2 and NH_3 incorporated into the liquid phase. We do not account for the charges brought by Na^+ and Cl^- in Equation (22), as their concentrations in Europa's ocean, particularly in its primordial state, remain poorly constrained. Moreover, the concentration ranges reported in the literature vary, depending on the composition of the rocky seafloor and the water-to-rock ratio, and these geochemical factors are beyond the scope of this paper.

These equations ensure the conservation of mass and charge within the H_2O–CO_2–NH_3 system. The resulting system of equations, coupling the liquid–vapor equilibrium and the chemical equilibrium, is solved using the Levenberg–Marquardt minimization method. This equation-solving process is highly sensitive to the initial guesses, so the model has been adjusted and benchmarked against UNIQUAC model results and experimental data from the literature (D. W. Van Krevelen et al. 1949; U. Gppert & G. Maurer 1988; V. Bieling et al. 1989; V. Darde et al. 2010).

Experimental data (D. W. Van Krevelen et al. 1949; U. Gppert & G. Maurer 1988; V. Bieling et al. 1989; V. Darde et al. 2010) and models (e.g., J. C. Castillo-Rogez et al. 2022) show that when CO_2 and NH_3 are present together in water, they can react to form ammonium carbamate (NH_2COO^-), as described in Equation (14). D. W. Van Krevelen et al. (1949) pointed out that below a certain ratio of total dissolved CO_2 to NH_3, m_{CO_2}/m_{NH_3} ~ [0.4–0.5]), ammonia can trap CO_2 in the liquid phase, preventing it from entering the gaseous phase. In this scenario, the dissolved CO_2 is converted into carbonate and bicarbonate ions (HCO_3^-, CO_3^{2-}; Equations (11) and (13)), which then react with ammonium (NH_4^+; Equation (12)) to form ammonium carbamate (NH_2COO^-; Equation (14)). However, above this threshold, a thick CO_2 atmosphere can be in equilibrium with the water ocean.

Table 3
Volatile Distributions from Cometary Building Blocks Adopted for the Primordial Outgassed Atmosphere (Expressed in Mole Fractions)

Molecule	Case 1a: 67P[a]	Case 1b: CO_2-rich Comet[b]
H_2O	9.18×10^{-1}	7.28×10^{-1}
CO_2	4.31×10^{-2}	2.18×10^{-1}
NH_3	6.15×10^{-3}	4.87×10^{-3}
O_2	2.84×10^{-2}	2.25×10^{-2}
CO	2.84×10^{-2}	2.25×10^{-2}
CH_4	3.12×10^{-3}	2.47×10^{-3}
N_2	8.17×10^{-4}	6.48×10^{-4}
Ar	5.32×10^{-6}	4.22×10^{-6}
Kr	4.50×10^{-7}	3.57×10^{-7}
Xe	2.20×10^{-7}	1.75×10^{-7}

Notes.
[a] M. Rubin et al. (2019).
[b] D. Bockelée-Morvan & N. Biver (2017).

3. Results

In the following, we investigate two different sets of initial conditions for our model. The first set explores the scenario where Europa's hydrosphere originates from the accretion of building blocks with a comet-like composition. The second set of initial conditions assumes that Europa's primordial hydrosphere formed in equilibrium with a thick, CO_2-rich atmosphere.

3.1. Hydrosphere Formation from Comet-like Building Blocks

Europa could have been partly formed from volatile-rich solids, presenting a cometary-like composition (R. M. Canup & W. R. Ward 2002; T. Ronnet et al. 2017; O. Mousis et al. 2023). The potential distribution of volatiles brought to Europa's hydrosphere can be assumed to span a range of comet compositions, as discussed in D. Bockelée-Morvan & N. Biver (2017).

The model described above is used to explore how the initial volatile dispatch, particularly the total dissolved CO_2/NH_3 ratio, can influence the partitioning of volatiles between the atmosphere and the ocean of early Europa and similar icy bodies.

We have applied the model to two different volatile distributions in the ice phase of comets, shown in Table 3. Case 1a is derived from data from Comet 67P/Churyumov–Gerasimenko (M. Rubin et al. 2019). Case 1b is an end-member composition, with the same gas distribution as 67P, except CO_2, which is set to the maximum fraction observed in comets (D. Bockelée-Morvan & N. Biver 2017). The calculation is done at a temperature of 300 K, which is a plausible surface temperature reached after accretion (C. J. Bierson & F. Nimmo 2020). The initial total pressure is approximated to be $P_{tot} = P^{sat}_{H2O}$, with water being the main constituent of the atmosphere right after accretion.

The resulting distribution of species at equilibrium between the two phases is shown in Figure 2. For the case in which

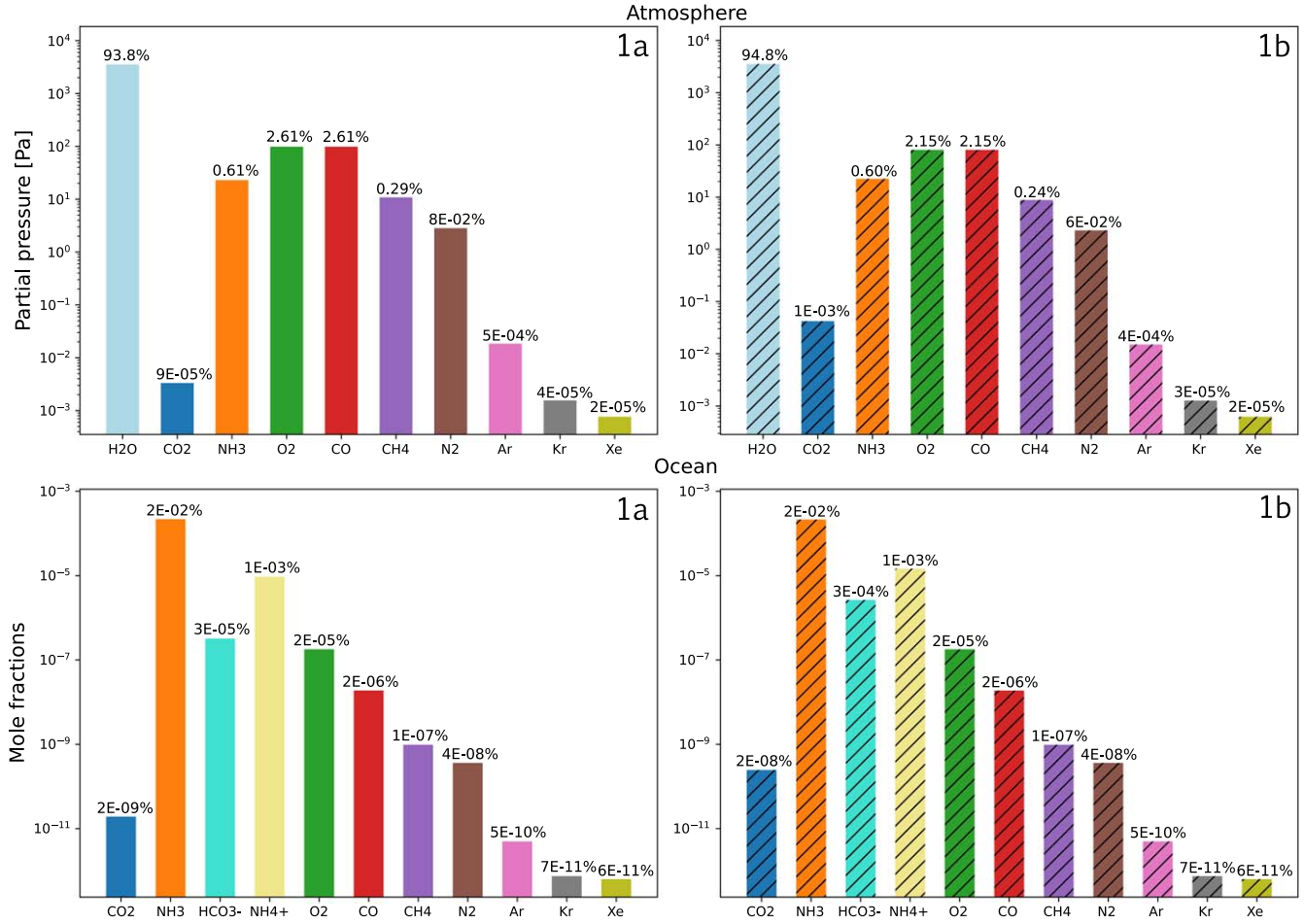

Figure 2. Volatile abundances at equilibrium in the primordial atmosphere and ocean of Europa at $T = 300$ K. Two initial distributions are considered: Case 1a (solid), based on the composition of Comet 67P; and Case 1b (hatched), derived from a high-CO_2 end-member composition. Final atmospheric fractions are expressed as partial pressures (Pascal), while dissolved volatile fractions are presented as mole fractions. The percentage share of each species in each phase is displayed above each vertical bar. The figure highlights only the two most abundant ions: HCO_3^- and NH_4^+.

Europa's hydrosphere formed from cometary ice, a significant fraction of ammonia is initially introduced into the primordial atmosphere. While carbon dioxide is initially the second most abundant component of the atmosphere after water vapor, its solubility in water is lower than that of ammonia. Consequently, a larger fraction of ammonia initially dissolves in the ocean compared to carbon dioxide when exposed to the atmosphere. Figure 2 shows that the consequence of this small total dissolved CO_2/NH_3 ratio is the scarce amount of CO_2 left in the atmosphere and dissolved in the ocean once chemical equilibrium is reached. The pH at the interface of the ocean at equilibrium is alkaline in both cases (pH ~10.5). Indeed, at such high pH, CO_2 is mostly retained as bicarbonate and carbonate ions.

To further highlight the influence of the initial atmospheric CO_2/NH_3 ratio on the distribution of volatiles in the primordial atmosphere, Figure 3 represents the sensitivity of the distribution of the molecules at $T = 300$ K to the variation of the fraction of NH_3 initially incorporated into the atmospheric interface. The fractions of CO_2 and other species initially incorporated into the gas phase are constant. y_{NH_3} is taken in the range of 10^{-8} to 6.15×10^{-3} (Table 3).

Figure 3 highlights the existence of a threshold on the initially accreted CO_2/NH_3 ratio at which most of the CO_2 is transformed, both in the atmosphere and in the ocean. Indeed, we compute that in our case, the share of NH_3 prevails over CO_2 in the atmosphere when initial $y^{ini}_{NH_3} > 10^{-4} \times y_{CO_2}$. As the initial fraction of NH_3 increases, so does the fraction of N-bearing ions, especially NH_2COO^-, which is formed from carbonate ions. In fact, the chemical reaction that forms NH_2COO^- is a thermodynamically favored reaction ($K_{NH_2COO^-} \sim 2$, whereas $K_{HCO_3^-} \sim 10^{-11}$ at 300 K). As the fraction of NH_3 increases, the concentration of HCO_3^- remains relatively constant, indicating that CO_2 is increasingly transformed to maintain chemical equilibrium. The figure shows that CO_2 and NH_3 cannot coexist as the primary atmospheric compounds simultaneously, as previously found by N. Marounina et al. (2018) in their study of Titan's primordial ocean. Their relative abundances exhibit an inverse relationship, where increasing the initial NH_3 abundance in the atmosphere leads to a corresponding decrease in CO_2. Furthermore, we can emphasize the relationship between this trend and the ocean's pH. As predicted by Equations (11)–(14), and as is visible in Figure 3, a higher CO_2/NH_3 ratio acidifies the ocean, while an increase of ammonia favors the formation of carbonates and a basic pH. Hence, the initially accreted CO_2/NH_3 ratio is a pivotal factor in the determination of the ocean's pH as well.

Figure 4 illustrates the impact of temperature on the chemical equilibrium shown in Case 1a, investigated over a range from 273.15 to 358 K. The upper limit of 358 K represents a plausible temperature that can be attained on Europa after accretion. We compute it using the approach

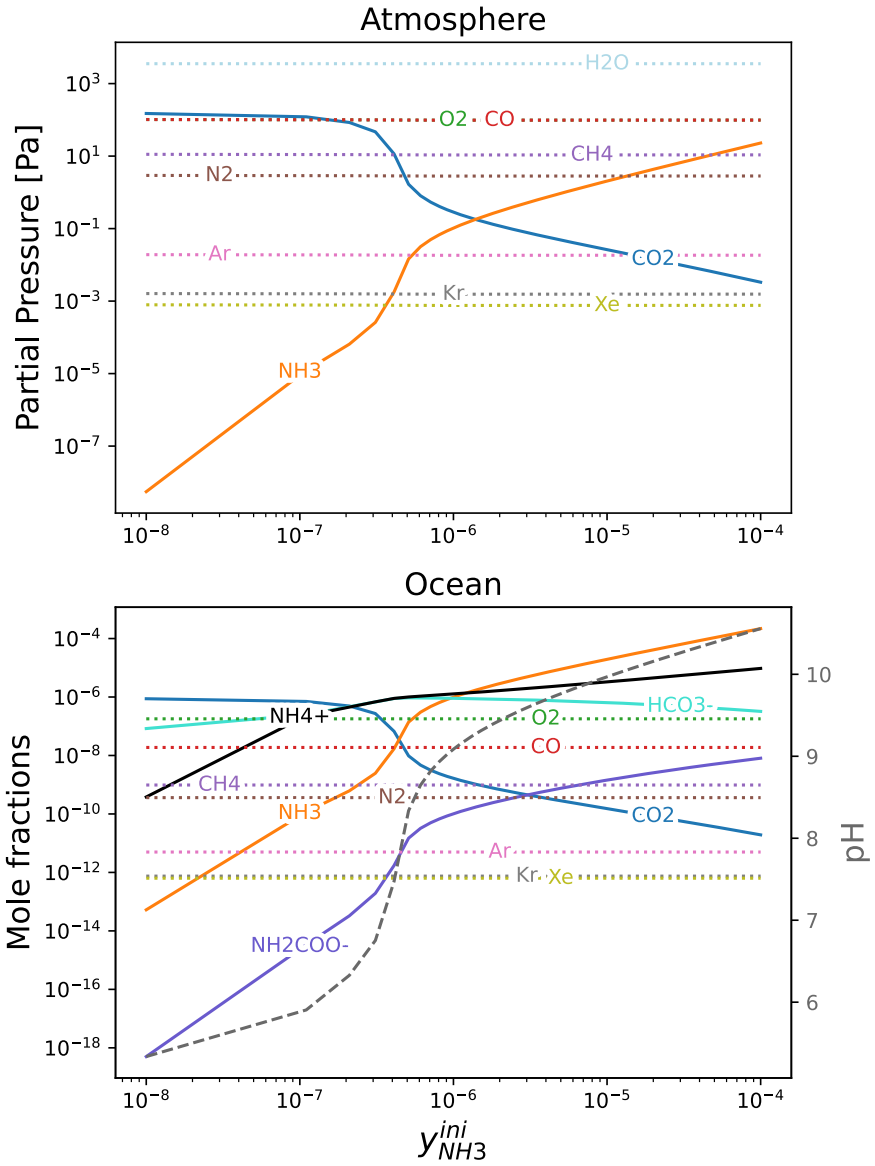

Figure 3. Evolution at $T = 300$ K of the final distribution of species in the atmosphere and ocean at equilibrium as a function of $y^{\mathrm{ini}}_{\mathrm{NH_3}}$, the initial mole fraction of NH_3 incorporated into the atmosphere. The initial mole fractions of all other species remain constant. Only the three most abundant ions—HCO_3^-, NH_4^+, and NH_2COO^-—are displayed in this figure. The dashed gray line corresponds to the pH of the ocean calculated as a function of $y^{\mathrm{ini}}_{\mathrm{NH_3}}$.

outlined in G. Schubert et al. (1981) and O. Grasset & C. Sotin (1996). This calculation considers Europa's kinetic energy from accretion, with a fraction h of this energy—specifically, $h = 0.1$—converted into heat.

The initial atmospheric pressure at the interface is approximated by the saturation vapor pressure of water. Figure 4 shows that as the initial pressure increases with temperature (O. C. Bridgeman & E. W. Aldrich 1964), the partial pressures of the various species also increase by about an order of magnitude in pressure between 273.15 and 358 K. However, due to temperature-dependent variations in Henry's constants, the mole fractions of the dissolved species, including the noble gases (tracers of the moon's evolution), show a slight decrease with temperature, less than an order of magnitude. However, CO_2 and NH_3 behave differently from the other species, because of the chemical reactions in which they are involved. In fact, with increasing temperature, CO_2 is less likely to be trapped by the formation of NH_2COO^-, because this chemical reaction is less thermodynamically favored with increasing temperature (K. Kawazuishi & J. M. Prausnitz 1987). Thus, at higher temperatures, a larger fraction of CO_2 remains in the atmosphere (more than 2 orders of magnitude in partial pressure between 273.15 and 357.6 K). Consequently, the partial pressure of NH_3 decreases slightly, and the mole fraction of the dissolved NH_3 lessens by an order of magnitude with increasing temperature.

3.2. Equilibrium with a Thick-and-CO_2-dominated Atmosphere

Here, it is assumed that Europa's primordial hydrosphere equilibrated with a thick-and-CO_2-rich atmosphere, based on the idea that the ocean could originate from a metamorphic origin (M. Melwani Daswani et al. 2021). As previously shown in Figure 3, the dominance of the partial pressure of carbon dioxide over that of ammonia, and vice versa, is determined by the accreted CO_2/NH_3 ratio in the ocean. Figure 5 illustrates

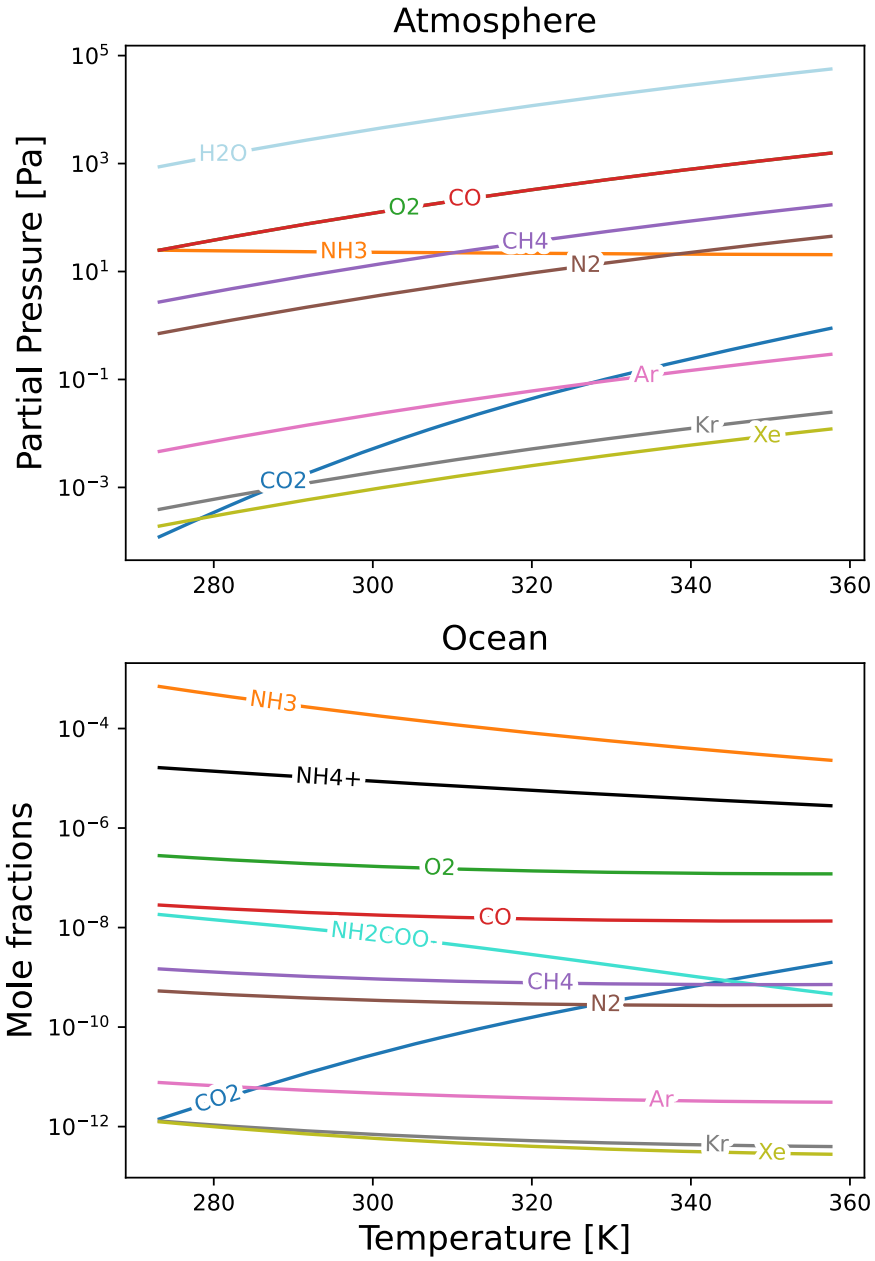

Figure 4. Evolution of final partial pressures and mole fractions in the ocean at equilibrium as a function of temperature. Not all dissolved ions in the ocean are displayed in the figure, even though they are present in the mixture.

the equilibrium state of the primordial hydrosphere for two initial atmospheric conditions: one with the partial pressure of CO_2 set to 1 bar (comprising 96.3% of the atmosphere; Case 2a) and another set to 10 bar (comprising 99.6% of the atmosphere; Case 2b). The initial partial pressure of water is set to the saturation vapor pressure of water, and the partial pressures of other species are calculated as fractions of this saturation vapor pressure, following the fractions provided by M. Rubin et al. (2019). The corresponding initial volatile fractions are listed in Table 4.

Starting with a high CO_2 fraction in the primordial atmosphere results in a higher fraction of total accreted CO_2 compared to NH_3. Consequently, such a configuration maintains a CO_2-rich primordial atmosphere at equilibrium. However, contrary to what is shown in Section 3.1, with the total dissolved CO_2/NH_3 ratio favoring CO_2, almost all NH_3 is transformed in both scenarios. The speciation of NH_3 in NH_4^+ and NH_2COO^- leads to a significantly reduced residual fraction of free NH_3 in both phases at equilibrium compared to the initial conditions in the primordial atmosphere.

Additionally, the higher the initial CO_2 partial pressure, the less CO_2 is removed from the atmosphere due to chemical equilibrium. When the initial P_{CO_2} is 1 bar, 40% of the initial CO_2 is sequestered in ionic forms in the ocean. In contrast, this percentage drops to nearly 0% when the initial P_{CO_2} is 10 bar. Unlike the cases studied in Table 3, the pH at the ocean–atmosphere interface resulting from this equilibrium is acidic, with pH values of 6.1 for Case 2a and 4.9 for Case 2b.

4. Discussion

The composition of Europa's current subsurface ocean remains poorly constrained (T. M. Becker et al. 2024).

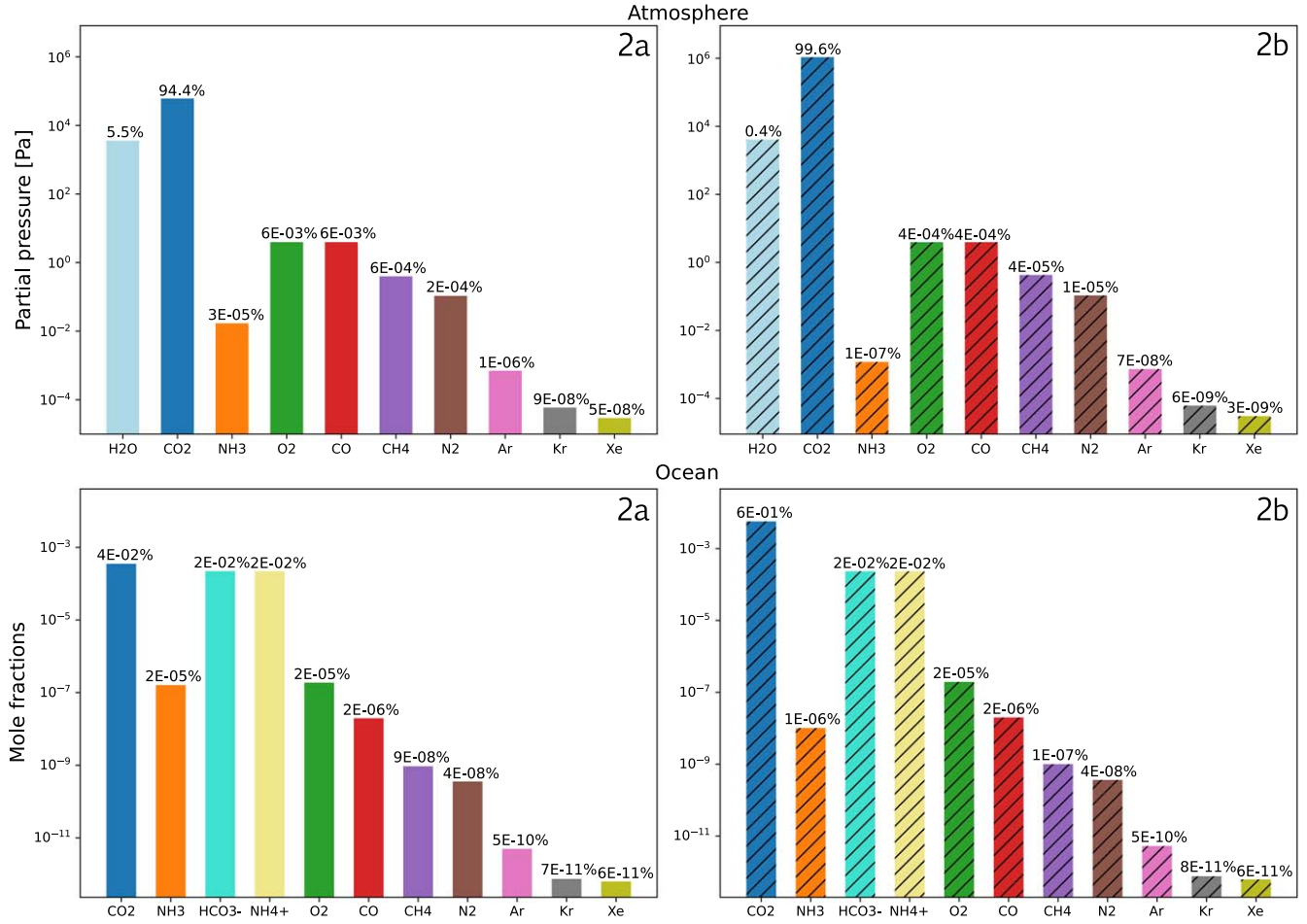

Figure 5. Volatile abundances at equilibrium in the primordial atmosphere and ocean of Europa at $T = 300$ K. Two initial distributions are considered: one with P_{CO_2} initially set to 1 bar (Case 2a, solid) and another with P_{CO_2} initially set to 10 bar (Case 2b, hatched). Atmospheric fractions are represented as partial pressures (Pascal), while dissolved volatile fractions are shown as mole fractions. The figure displays only the two most abundant ions, HCO_3^- and NH_4^+.

Table 4
Adopted Volatile Distributions in the Primordial Atmospheric Reservoir, Assuming Equilibration with a CO_2-rich Atmosphere (Expressed in Mole Fractions)

Molecule	Case 2a: $P_{CO_2} = 1$ bar	Case 2b: $P_{CO_2} = 10$ bar
H_2O	3.42×10^{-2}	3.36×10^{-3}
CO_2	9.63×10^{-1}	9.96×10^{-1}
NH_3	2.23×10^{-4}	2.40×10^{-5}
O_2	1.11×10^{-3}	1.10×10^{-4}
CO	1.11×10^{-3}	1.10×10^{-4}
CH_4	1.12×10^{-4}	1.20×10^{-5}
N_2	3.00×10^{-5}	3.00×10^{-6}
Ar	1.98×10^{-7}	2.05×10^{-8}
Kr	1.67×10^{-8}	1.73×10^{-9}
Xe	8.22×10^{-9}	8.50×10^{-10}

However, surface observations in recent years have provided insights into the variety of species present within the ocean (N. Ligier et al. 2016; C. Hibbitts et al. 2019; S. K. Trumbo & M. E. Brown 2023; G. L. Villanueva et al. 2023). The concentration ranges of these dissolved species are uncertain, and models depend on only partially understood physical variables, such as pH, salinity, and rock composition. Furthermore, due to the potential role of the radiolytic oxidation of organics on Europa's surface, assessing the extent of the aqueous alteration of compounds like CO_2 is challenging (M. Y. Zolotov 2012), which in turn complicates the estimation of the amount of carbonates present in the ocean. Although it was targeted, the carbonate content could not be estimated by S. K. Trumbo & M. E. Brown (2023) or G. L. Villanueva et al. (2023).

Our study uncovers the implications of several formation scenarios on the state of the primordial hydrosphere, particularly regarding the distribution of ionic compounds resulting from the speciation of CO_2 and NH_3. Current knowledge of Europa's subsurface ocean does not allow us to favor one end-member scenario over another regarding its primordial hydrosphere composition. However, M. Y. Zolotov et al. (2009) modeled examples of Europa's ocean composition based on the ocean's pH and redox state, demonstrating that the pH is highly dependent on the types of rocks (e.g., chondritic, basaltic) exposed to water.

It is also important to emphasize that the type and quantity of dissolved gases influence the ocean's pH (see Figure 3), as predicted by thermodynamic principles. Our computations indicate that when CO_2 is primarily sequestered as carbonates due to high NH_3 concentrations, the ocean maintains a basic pH at equilibrium (Cases 1a and b). In contrast, when in equilibrium with a thick-and-CO_2-rich atmosphere (Cases 2a and b), the ocean exhibits a more acidic pH.

As highlighted by geochemical models, the water-to-rock ratio and the reactivity of nonvolatile compounds are crucial in

determining the ocean's pH. M. Y. Zolotov (2012) noted that when the igneous rocks of the silicate mantle are exposed to water, the types of minerals subject to dissolution—and thus involved in the ocean's chemistry—depend on whether the ocean is in acidic or alkaline conditions. In an alkaline environment, CO_2 can be converted into carbonates and bicarbonates (Cases 1a and b), which may eventually precipitate. However, as demonstrated by M. Y. Zolotov (2012), carbonate concentrations could be influenced by the presence of ions such as Ca^{2+}, allowing for other components to impact the CO_2–NH_3 chemical equilibrium via

$$2HCO_3^- + Ca^{2+} \rightleftharpoons CaCO_3 + H_2O + CO_2, \quad (23)$$

$$CO_3^{2-} + Ca^{2+} \rightleftharpoons CaCO_3. \quad (24)$$

On the other hand, salinity can play a key role in determining the concentration of precipitated solutes, which in turn affects the pH. J. C. Castillo-Rogez et al. (2022) emphasized that the presence of carbonates and other ions resulting from the equilibrium between CO_2, NH_3, and rocks can also influence the salinity and conductivity of the ocean. These parameters may have been impacted by changes in the thickness of the icy shell over time as well (H. Melosh et al. 2004). Although extreme fluctuations are unlikely, due to the presence of buffering agents (P. V. Johnson et al. 2019), the current state of knowledge regarding the ocean's composition does not permit a reliable assessment of Europa's oceanic pH (T. M. Becker et al. 2024). Without this information, we are unable to constrain the CO_2/NH_3 ratio.

Future measurements are needed to better assess the state of Europa's subsurface ocean. As highlighted by G. L. Villanueva et al. (2023) and S. K. Trumbo & M. E. Brown (2023), observations of surface features and spectral analyses can test the endogenic origin of species detected through remote sensing. If future space missions identify plumes on Europa's surface, in situ measurements could provide direct data on materials originating from the ocean, similar to what Cassini accomplished with the Enceladus plumes (F. Postberg et al. 2009, 2011; J. H. Waite et al. 2017; C. Glein et al. 2018; C. Hansen et al. 2020).

Specifically, in situ data from Europa Clipper's SUDA and MASPEX instruments (J. H. Waite et al. 2024), along with JUICE's Particle Environment Package (PEP) instrument, will offer valuable insights into ions such as HCO_3^- and CO_3^{2-}, which are pertinent to our study, as well as neutral species present in the ocean (M. Föhn et al. 2021; T. M. Becker et al. 2024). These measurements could be complemented by remote-sensing analyses from Clipper's Europa-UVS instrument to gather additional information on volatiles. By integrating data on CO_2 from MASPEX and PEP and carbonates from SUDA, we could constrain the primordial CO_2/NH_3 inventory thanks to our model. Thus, modeling the relationship between the current and primordial states of Europa's ocean will enable more accurate estimates of the relative abundances of specific species (especially CO_2 and NH_3), helping to differentiate between competing end-member scenarios based on the results of this study.

5. Summary and Conclusions

Our work provides an initial assessment of the distribution of primordial volatiles in Europa's early hydrosphere, considering the liquid–vapor equilibrium at the atmosphere–ocean interface and the chemical equilibrium within the ocean. To do so, we have assumed that the atmospheric reservoir outgassed from the interior due to vigorous accretional and radiogenic heating, reaching equilibrium with an underlying liquid ocean. We show how the initial NH_3 proportion in Europa's building blocks could influence the primordial atmospheric CO_2 distribution. In Case 1, the initial volatile atmospheric distribution was based on cometary abundances. We demonstrate that at 300 K, the primordial hydrosphere at equilibrium is CO_2-depleted, despite a significant fraction being delivered to the early atmosphere. By varying the initial NH_3 fraction, we observe that a CO_2-rich atmosphere could be sustained above a certain CO_2/NH_3 threshold. However, in Case 2, the initial primordial atmosphere's composition is CO_2-rich. We have shown that starting from such a configuration, the primordial atmosphere retains a significant CO_2 proportion at equilibrium, while NH_3 is transformed in the liquid phase. Overall, we highlight, studying these two cases, the significance of the initially accreted CO_2/NH_3 ratios on their partial pressure distributions at equilibrium in the primordial atmosphere. The proportion of CO_2 in the atmosphere is correlated to the value of this ratio, which can lead to a depletion of multiple orders of magnitude in partial pressure when it is below the threshold. This conclusion relates to the amount of NH_3 that could have initially been incorporated into Europa's hydrosphere, which may have helped keep the ocean liquid due to its antifreeze properties (M. Neveu et al. 2017). However, the required NH_3 abundance must be balanced against the CO_2 quantity needed to match present-day abundances (S. K. Trumbo & M. E. Brown 2023; G. L. Villanueva et al. 2023). A significant concentration of dissolved NH_3 (greater than 5%) is required to effectively lower the freezing point of the ocean (G. Tobie et al. 2012). Should future measurements indicate a substantial fraction of free CO_2 dissolved in the ocean, this will impose an upper limit on NH_3 concentration, based on the results of this study. Therefore, if the NH_3 concentration falls below the threshold necessary for a significant antifreeze effect, the antifreeze contribution for maintaining the ocean in a liquid state may need to be reconsidered.

In the presence of a significant amount of NH_3, the likely consequence, depending on the counterions available, is that a significant amount of these carbonates will precipitate, accentuating the suppression of CO_2. The work of C. R. Glein & J. H. Waite (2020) on Enceladus has shown that the carbonate content of the ocean can be strongly influenced by the balance between the ocean and seafloor alteration minerals. M. Melwani Daswani et al. (2021) also explored how rock devolatilization and aqueous alteration, taking into account carbonate precipitation, can lead to a thick CO_2 primordial atmosphere for Europa. However, NH_3 has not been included in these models, and we have shown that its presence can shift the resulting equilibrium. It is therefore crucial to further couple this model with a geochemical model to explore how exchanges between the rocky bottom of Europa's ocean may affect its composition. In addition, as a consequence of the extraction of elements from the silicate mantle, additional species may be introduced into the ocean and affect the latter's equilibrium as well (M. Y. Zolotov & E. L. Shock 2001; S. D. Vance et al. 2016), including the nature and amount of antifreeze, such as NH_3 (M. Neveu et al. 2017). Although we have only considered the chemical reactions involving CO_2 and NH_3 in this model, more chemistry should be considered in the case of hydrothermal processes. Indeed, J. S. Seewald et al.

(2006) have shown that reduced carbon compounds could be formed under these conditions, with CO_2, CH_3OH, and CO as major or trace components.

One should note that this study's model focuses on the primordial ocean–atmosphere interaction. Moreover, the atmosphere considered in this model is isothermal and without escape. Such assumptions limit the accuracy of the model, since volatile species such as CO and CH_4 are present. Atmospheric escape would profoundly affect the hydrosphere equilibrium, depleting the atmosphere of volatiles. In addition, the greenhouse effect that could be produced by the gas has not been included. However, our model provides an upper limit on the partial pressures reached in the atmosphere without escape, for the most volatile species released by the building blocks after accretion.

Additionally, the formation of clathrate hydrates should be considered under the following conditions:

1. If an additional source of volatiles raises the concentration in the ocean above the solubility limit, leading to bubble formation.
2. If the pressure of the gaseous mixture in the bubbles exceeds the dissociation pressure of the corresponding clathrate hydrate.

Clathrate hydrates could serve as another volatile reservoir, influencing the composition of the primordial atmosphere over time (O. Prieto-Ballesteros et al. 2005; M. Y. Zolotov et al. 2009; O. Mousis et al. 2013; A. Bouquet et al. 2019). If the density of clathrate hydrates is lower than that of the ocean, they can float to the surface, forming a crustal layer that affects the exchange between the liquid and gaseous phases (O. Prieto-Ballesteros et al. 2005; N. Marounina et al. 2018; K. Kalousová & C. Sotin 2020). The buoyancy of clathrates can be influenced by the ocean's salinity and composition (O. Prieto-Ballesteros et al. 2005), highlighting the importance of coupling a self-consistent, time-dependent model of clathrate hydrate formation with the one presented in this paper.

Our work provides a first assessment of the distribution of primordial volatiles in Europa's primitive hydrosphere. The Europa Clipper mission will be able to measure the current composition of Europa's hydrosphere. By combining these measurements with future modeling, it will be possible to derive the composition of the primordial hydrosphere and compare it with the predictions of our model, providing insight into the conditions under which Europa formed.

Acknowledgments

O.M. and A.B. acknowledge support from CNES. The project leading to this publication has received funding from the Excellence Initiative of Aix-Marseille Université—A*Midex, a French "Investissements d'Avenir" program, AMX-21-IET-018. This research is part of the project FACOM (ANR-22-CE49-0005-01 ACT) and has benefited from funding provided by l'Agence Nationale de la Recherche (ANR) under the Generic Call for Proposals 2022. The work of C.R.G. was supported by NASA's Preparatory Science Investigations for Europa (PSIE) program.

ORCID iDs

Alizée Amsler Moulanier https://orcid.org/0009-0000-7492-1476
Olivier Mousis https://orcid.org/0000-0001-5323-6453
Alexis Bouquet https://orcid.org/0000-0001-8262-9678

References

Becker, T. M., Zolotov, M. Y., Gudipati, M. S., et al. 2024, SSRv, 220, 49
Bieling, V., Rumpf, B., Strepp, F., & Maurer, G. 1989, FlPEq, 53, 251
Bierhaus, E. B., Zahnle, K., Chapman, C. R., & Dotson, R. 2009, in Europa, ed. R. T. Pappalardo, W. B. McKinnon, & K. K. Khurana (Tucson, AZ: Univ. Arizona Press), 161
Bierson, C. J., & Nimmo, F. 2020, ApJ, 897, L43
Bockelée-Morvan, D., & Biver, N. 2017, RSPTA, 375, 20160252
Bouquet, A., Mousis, O., Glein, C. R., Danger, G., & Waite, J. H. 2019, ApJ, 885, 14
Bridgeman, O. C., & Aldrich, E. W. 1964, ATJHT, 86, 279
Canup, R. M., & Ward, W. R. 2002, AJ, 124, 3404
Castillo-Rogez, J. C., Daswani, M. M., Glein, C. R., Vance, S. D., & Cochrane, C. J. 2022, GeoRL, 49, e2021GL097256
Dalton, J., Prieto-Ballesteros, O., Kargel, J., et al. 2005, Icar, 177, 472
Darde, V., Van Well, W. J. M., Stenby, E. H., & Thomsen, K. 2010, Ind. Eng. Chem. Res., 49, 12663
Dhima, A., De Hemptinne, J.C., & Jose, J. 1999, Ind. Eng. Chem. Res., 38, 3144
Föhn, M., Galli, A., & Vorburger, A. 2021, Description of the Mass Spectrometer for the Jupiter Icy Moons Explorer Mission in 2021 IEEE Aerospace Conf. (IEEE: Piscataway, NJ)
Garcia, J. E. 2001, Density of Aqueous Solutions of CO2 LBNL-49023; R&D Project: 468111; TRN: US200806%%85 Lawrence Berkeley National Laboratory
Gasem, K., Gao, W., Pan, Z., & Robinson, R. 2001, FlPEq, 181, 113
Glein, C., Postberg, F., & Vance, S. 2018, The Geochemistry of Enceladus: Composition and Controls, Enceladus and the Icy Moons of Saturn (Tucson, AZ: Univ. Arizona Press), 39
Glein, C. R., & Waite, J. H. 2020, GeoRL, 47, e2019GL085885
Gomez Casajus, L., Zannoni, M., Modenini, D., et al. 2021, Icar, 358, 114187
Grasset, O., & Sotin, C. 1996, Icar, 123, 101
Gppert, U., & Maurer, G. 1988, FlPEq, 41, 153
Hansen, C., Esposito, L., Colwell, J., et al. 2020, Icar, 344, 113461
Hibbitts, C., Stockstill-Cahill, K., Wing, B., & Paranicas, C. 2019, Icar, 326, 37
Johnson, P. V., Hodyss, R., Vu, T. H., & Choukroun, M. 2019, Icar, 321, 857
Kalousová, K., & Sotin, C. 2020, GeoRL, 47, e2020GL087481
Kawazuishi, K., & Prausnitz, J. M. 1987, Ind. Eng. Chem. Res., 26, 1482
Khurana, K. K., Kivelson, M. G., Stevenson, D. J., et al. 1998, Natur, 395, 777
Kivelson, M. G., Khurana, K. K., Russel, C. T., et al. 2000, Sci, 289, 1340
Kvamme, B. 2021, Fluid, 6, 345
Ligier, N., Poulet, F., Carter, J., Brunetto, R., & Gourgeot, F. 2016, AJ, 151, 163
Lunine, J. I., & Nolan, M. C. 1992, Icar, 100, 221
Lunine, J. I., & Stevenson, D. J. 1987, Icar, 70, 61
Marion, G., Kargel, J., Catling, D., & Lunine, J. 2012, Icar, 220, 932
Marounina, N., Grasset, O., Tobie, G., & Carpy, S. 2018, Icar, 310, 127
McCord, T. B., Teeter, G., Hansen, G. B., Sieger, M. T., & Orlando, T. M. 2002, JGRE, 107, 4
Melosh, H., Ekholm, A., Showman, A., & Lorenz, R. 2004, Icar, 168, 498
Melwani Daswani, M., Vance, S. D., Mayne, M. J., & Glein, C. R. 2021, GeoRL, 48, e2021GL094143
Mousis, O., & Gautier, D. 2004, P&SS, 52, 361
Mousis, O., Lakhlifi, A., Picaud, S., Pasek, M., & Chassefire, E. 2013, AsBio, 13, 380
Mousis, O., Schneeberger, A., Lunine, J. I., et al. 2023, ApJL, 944, L37
Neveu, M., Desch, S. J., & Castillo-Rogez, J. C. 2017, GeCoA, 212, 324
Pappalardo, R. T., Belton, M. J. S., Breneman, H. H., et al. 1999, JGR, 104, 24015
Pappalardo, R. T., Buratti, B. J., Korth, H., et al. 2024, SSRv, 220, 40
Pazuki, G., Pahlevanzadeh, H., & Ahooei, A. M. 2006, FlPEq, 242, 57
Peng, D.-Y., & Robinson, D. B. 1976, Industrial & Engineering Chemistry Fundamentals, 15, 59
Pizzarello, S., & Williams, L. B. 2012, ApJ, 749, 161
Postberg, F., Kempf, S., Schmidt, J., et al. 2009, Natur, 459, 1098
Postberg, F., Schmidt, J., Hillier, J., Kempf, S., & Srama, R. 2011, Natur, 474, 620
Prieto-Ballesteros, O., Kargel, J. S., Fernndez-Sampedro, M., et al. 2005, Icar, 177, 491
Prinn, R. G., & Fegley, B. J. 1981, ApJ, 249, 308
Reid, R., Prausnitz, J. M., & Poling, B. 1987, The Properties of Gases & Liquids: 4th Edition (New York: McGraw-Hill)

Ronnet, T., Mousis, O., & Vernazza, P. 2017, ApJ, 845, 92
Ronnet, T., Mousis, O., Vernazza, P., Lunine, J. I., & Crida, A. 2018, AJ, 155, 224
Rubin, M., Altwegg, K., Balsiger, H., et al. 2019, MNRAS, 489, 594
Rumpf, B., & Maurer, G. 1993a, BBGPC, 97, 85
Rumpf, B., & Maurer, G. 1993b, Ind. Eng. Chem. Res., 32, 1780
Schubert, G., Spohn, T., & McKinnon, W. B. 2004, Interior Composition, Structure and Dynamics of the Galilean Satellites, in Jupiter. The Planet, Satellites and Magnetosphere, ed. F. Bagenal, T. E. Dowling, & W. B. McKinnon, Vol. 1 (Cambridge: Cambridge Univ. Press), 281
Schubert, G., Stevenson, D., & Ellsworth, K. 1981, Icar, 47, 46
Seewald, J. S., Zolotov, M. Y., & McCollom, T. 2006, GeoCoA, 70, 446
Stull, D. R. 1947, Industrial & Engineering Chemistry, 39, 517
Thomsen, K. 2005, PApCh, 77, 531
Thomsen, K., & Rasmussen, P. 1999, ChEnS, 54, 1787
Tobie, G., Gautier, D., & Hersant, F. 2012, ApJ, 752, 125
Trinh, K. T., Bierson, C. J., & O'Rourke, J. G. 2023, SciA, 9, eadf3955
Trumbo, S. K., & Brown, M. E. 2023, Sci, 381, 1308
Van Krevelen, D.W., Hoftijzer, P. J., & Huntjens, F. J. 1949, Recueil des Travaux Chimiques des Pays-Bas, 68, 191
Vance, S. D., Hand, K. P., & Pappalardo, R. T. 2016, GeoRL, 43, 4871
Villanueva, G. L., Hammel, H. B., Milam, S. N., et al. 2023, Sci, 381 1305
Vrabec, J., Huang, Y.L., & Hasse, H. 2009, FlPEq, 279, 120
Waite, J. H., Glein, C. R., Perryman, R. S., et al. 2017, Sci, 356, 155
Waite, J. H., Burch, J. L., Brockwell, T. G., et al. 2024, SSRv, 220, 30
Warneck, P., & Williams, J. 2012, The Atmospheric Chemists Companion: Numerical Data for Use in the Atmospheric Sciences (Dordrecht: Springer)
Zolotov, M. Y. 2012, Icar, 220, 713
Zolotov, M. Y., Kargel, J. S., & Dotson, R. 2009, in Europa, ed. R. T. Pappalardo, W. B. McKinnon, & K. K. Khurana (University of Arizona Press), 431
Zolotov, M. Y., & Shock, E. L. 2001, JGR, 106, 32815